

# Emergence of spatiotemporal patterns in a fuel-driven coupled cooperative supramolecular system <sup>†</sup>

Akta Singh<sup>a</sup>, Nayana Mukherjee<sup>b</sup>, Jagannath Mondal<sup>a,\*</sup> and Pushpita Ghosh<sup>c,\*</sup>

Chemically fueled supramolecular systems can exhibit complex, time-dependent behaviors reminiscent of living matter when maintained far from equilibrium by continuous energy or fuel consumption. Here, we introduce a minimal reaction-diffusion model that captures the essential dynamics of a cooperative supramolecular polymerization network driven by monomer activation and deactivation. We show that a balance between autocatalytic growth and inhibitory decay sustains a nonequilibrium steady state in the model that undergoes a Hopf bifurcation, giving rise to autonomous oscillations. When spatial transport is introduced through diffusion, the system displays rich spatiotemporal phenomena, such as traveling wavefronts and transient polygonal patterns. Our results demonstrate that the interplay between reaction kinetics and diffusion can spontaneously generate self-organized, life-like dynamics in synthetic supramolecular polymer systems. This theoretical framework not only bridges molecular self-assembly and active matter dynamics but also provides design principles for creating adaptive, oscillatory, and self-patterning materials powered by chemical fuels.

## 1 Introduction

Self-organization and pattern formation are hallmarks of systems maintained far from thermodynamic equilibrium. Such processes are ubiquitous in nature from morphogenesis to intracellular organization and arise from nonlinear coupling between reaction kinetics, energy input, and spatial transport<sup>1–5</sup>. Living cells exemplify this principle: through continuous fuel consumption, they sustain non-equilibrium steady states (NESS) that drive complex behaviors such as oscillations, waves, and compartmentalization<sup>6–8</sup>. Cytoskeletal filaments such as actin and microtubules undergo ATP- or GTP-fueled polymerization-depolymerization cycles that enable dynamic reorganization and spatiotemporal patterning<sup>9–14</sup>.

Inspired by biological nonequilibrium systems, chemists have developed artificial supramolecular assemblies that are transiently sustained by chemical fuel<sup>15–23</sup>. In these systems, monomers are activated by a chemical or redox fuel to assemble into higher-order structures and subsequently deactivated to disassemble, leading to self-assembly under continuous turnover of components<sup>18,19,24</sup>. These fuel-driven reaction cycles embody the essence of *dissipative self-assembly*, where structural order is maintained only by ongoing energy dissipation<sup>25–27</sup>.

Remarkably, recent experiments have revealed that chemically fueled supramolecular systems can exhibit collective dynamics that transcend simple assembly-disassembly equilibria. Hermans and co-workers demonstrated a redox-driven supramolecular polymer that undergoes autonomous oscillations and produces traveling fronts and centimeter-scale patterns<sup>19</sup>. Related

studies have shown oscillatory force generation in supramolecular nanofiber networks<sup>29</sup>, spatiotemporal control of self-assembly using gradients or feedback<sup>30–32</sup>, and active supramolecular hydrogels exhibiting distinct network morphologies and pattern transitions<sup>33–35</sup>. Together, these studies reveal the potential for supramolecular polymers to serve as synthetic analogues of biological active matter.

In parallel, theoretical efforts in systems chemistry and soft active matter have emphasized that feedback-driven reaction networks coupled with spatial transport can give rise to oscillations, waves, and phase-separated morphologies<sup>7,18,26</sup>. Such frameworks bridge chemical kinetics and physics of pattern formation, offering insights into how molecular-level energy transduction can scale up to mesoscale order. However, despite growing experimental and theoretical progress, a quantitative and mechanistic understanding of how chemically fueled supramolecular polymers generate oscillations and spatial structures is still lacking. In particular, it remains unclear how molecular scale assembly kinetics can couple to transport to produce robust, life-like patterns without external control or fine-tuning.

Here, we develop a minimal reaction-diffusion model that captures the essential kinetic features of a chemically fueled, cooperative supramolecular polymerization system. The model unifies monomer activation-deactivation cycles with autocatalytic polymer growth and fragmentation, sustained by constant fuel flux. Linear stability analysis reveals the onset of temporal oscillations via a Hopf bifurcation, while the inclusion of spatial diffusion generates traveling polymerization fronts and transient polygonal patterns. This framework provides mechanistic insight into how feedback between nonequilibrium reaction kinetics and spatial transport can spontaneously generate life-like spatiotemporal organization in synthetic supramolecular systems.

## 2 Model Description

To establish a baseline for the spatiotemporal dynamics observed later, we first analyze the temporal behavior of the spatially ho-

<sup>a</sup> Tata Institute of Fundamental Research Hyderabad, Telangana 500046, India

<sup>b</sup> Department of Mathematics, Mahindra University, Hyderabad, Telangana 500043, India

<sup>c</sup> School of Chemistry, IISER Thiruvananthapuram, Kerala 695551, India

\* pushpita@iisertvm.ac.in, jmondal@tifrh.res.in

† Supplementary Information available: [details of any supplementary information available should be included here]. See DOI: 00.0000/00000000.

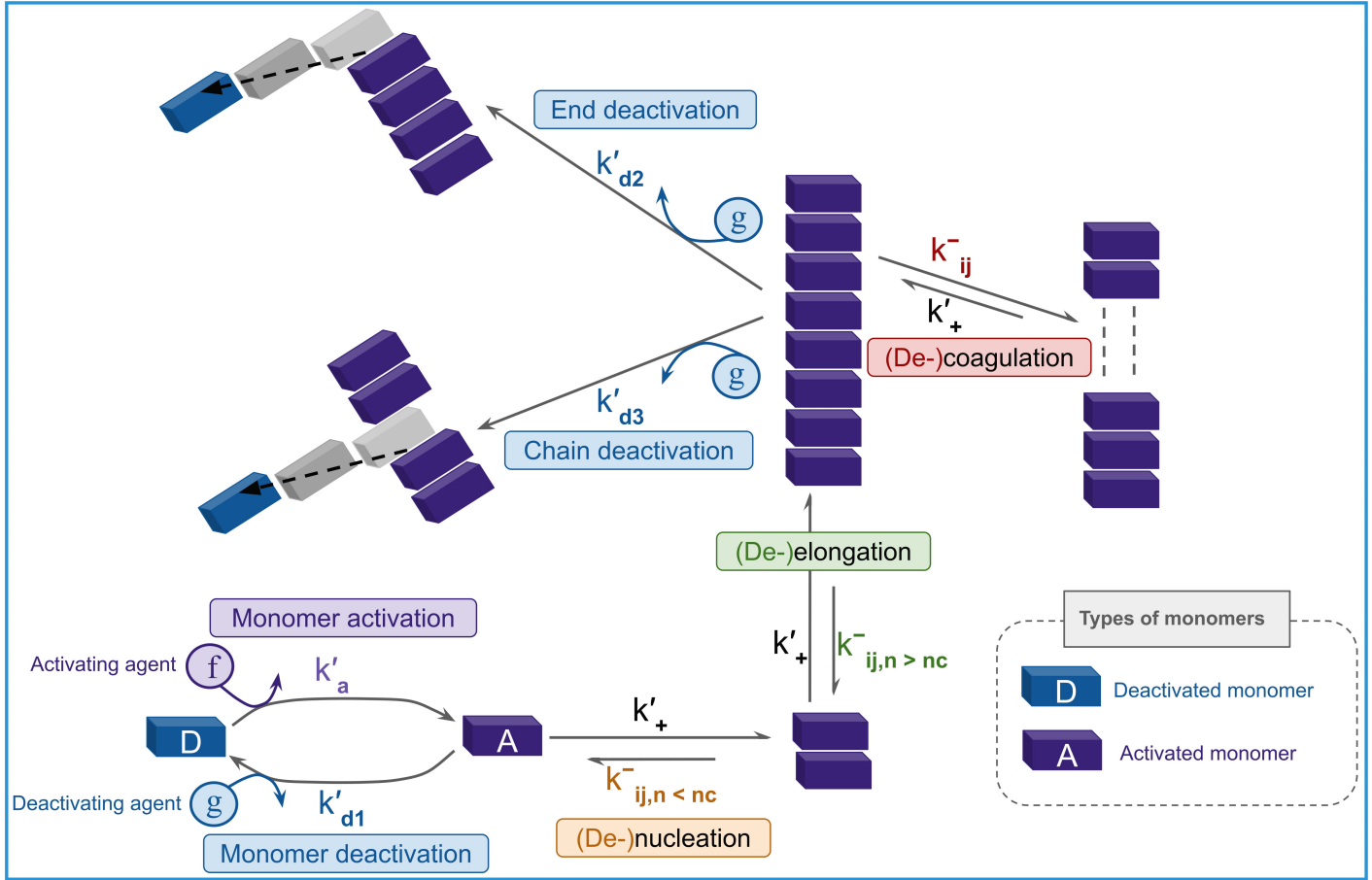


Fig. 1 Schematic of the coupled cooperative supramolecular polymerization model<sup>28</sup>. Constant supplies of activating (*f*) and deactivating (*g*) agents drive monomer activation/deactivation, polymer assembly (nucleation, elongation, coagulation), and disassembly (fragmentation and deactivation) under non-equilibrium conditions.

mogeneous (well-mixed) system, where diffusion is neglected. We adopt a coupled cooperative supramolecular polymerization model originally proposed by Sharko *et al.*<sup>28</sup>, schematically illustrated in Fig. 1. The model describes supramolecular self-assembly in a chemically fueled environment, where monomers undergo activation and deactivation while polymerization proceeds through nucleation, elongation, and coagulation (polymer-polymer fusion), together with their reverse steps: denucleation, de-elongation, and fragmentation. Constant concentrations of activating and deactivating agents (*f* and *g*) maintain the system in a non-equilibrium steady state. Polymer fragmentation provides a positive feedback: breaking fibers increases the number of free chain ends which act as growth sites. Conversely, monomer deactivation and polymer end-deactivation act as negative feedback, tending to halt growth. These built-in feedback loops are analogous to those identified experimentally (fragmentation vs. size-dependent depolymerization) as necessary for oscillations.

Monomer activation and deactivation are governed by pseudo-first-order rate constants  $k'_a$  and  $k'_{d1,2,3}$ , which depend on fuel concentrations and the local environment (free, chain-end, or internal monomer). The smallest stable nucleus consists of two monomers ( $n_c = 2$ ). All assembly processes share a rate constant  $k_+$ , while disassembly occurs through distinct pathways charac-

terized by rate constants  $k^-_{ij}$ .

The time evolution of the system is tracked through the concentrations of deactivated monomers  $d(t)$ , activated monomers  $a_1(t)$ , and two polymer moments: the total number concentration  $m'_0(t) = \sum_{n=2}^{\infty} a_n(t)$  and the total polymerized mass  $m'_1(t) = \sum_{n=2}^{\infty} n a_n(t)$  representing the total polymer chain count and total polymerized monomer, respectively. To simplify the model, only the dominant kinetic processes contributing to the evolution of these four variables are retained, yielding a reduced set of equations (Eqs. 1-4). The simplified model depends on the total monomer concentration  $c_{\text{tot}}$ , assembly rate constant  $k_+$ , activation rate  $k'_a$ , and deactivation rates  $k'_{d2}$  (end) and  $k'_{d3}$  (chain).

The system is rendered dimensionless by setting  $k_+ = K = 1$ , where  $K$  is the equilibrium dissociation constant, so that the concentration and time units are  $K$  and  $(k_+ K)^{-1}$ , respectively. For  $C = 4.6$ , Sharko *et al.*<sup>28</sup> showed that the simplified model reproduces the dynamics of the original formulation:

$$\dot{d} = -k'_a d + 2k'_{d2} m'_0 \quad (1)$$

$$\dot{a}_1 = k'_a d - 2k_+ a_1 m'_0 \quad (2)$$

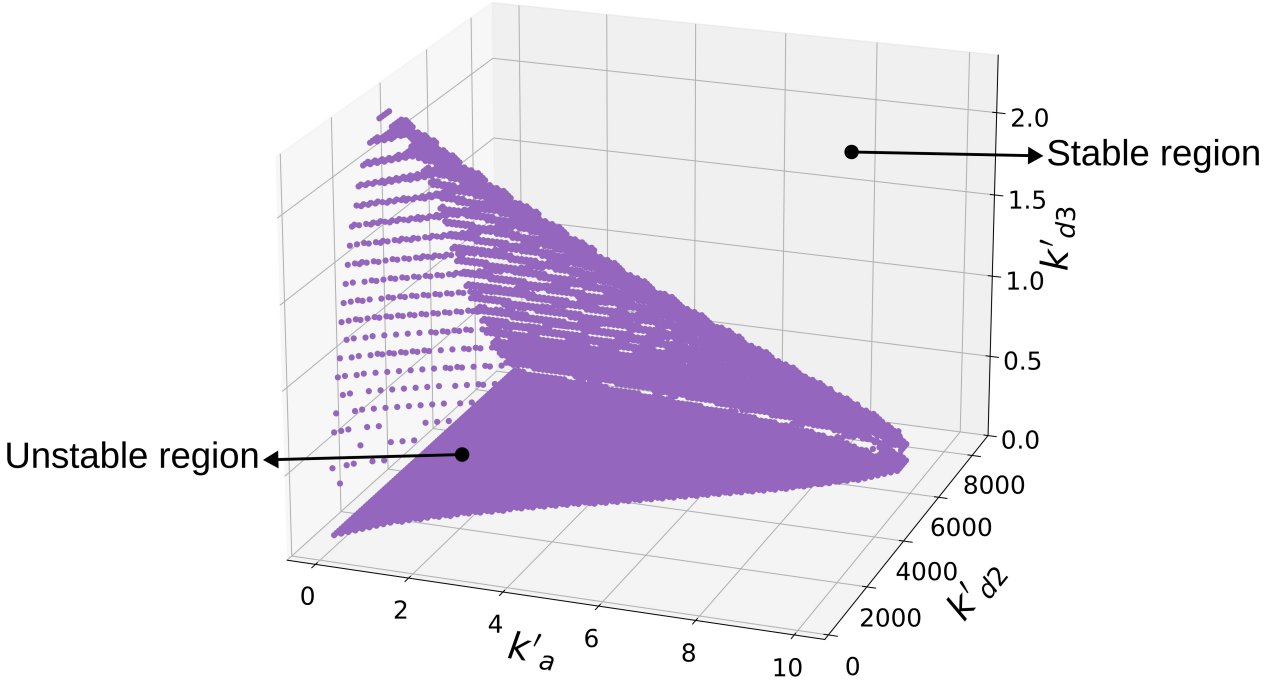


Fig. 2 Bifurcation diagram in the three-dimensional parameter space defined by  $k'_a$ ,  $k'_d2$ , and  $k'_d3$ , obtained numerically using linear stability analysis of the 3-component reduced system (SI, Section-1). The bifurcation surface, shown as purple dots, separates the parameter space into linearly stable and unstable regions.

$$\dot{m}'_1 = -2k'_d2m'_0 + 2k_+a_1m'_0 \quad (3)$$

$$\dot{m}'_0 = k'_d3(m'_1 - 4m'_0) - \frac{2k'_d2Cm'_0}{(m'_1/m'_0 - 2)^2} - 2k'_d3m'_0 - k_+(m'_0)^2 \quad (4)$$

### 3 Results and Discussion

#### 3.1 Identifying the conditions for temporal oscillations

Under certain conditions, the well-mixed (spatially uniform) version of this model exhibits self-sustained oscillations in time. By performing a linear stability analysis of the kinetic equations (details are provided in Methods section and Supporting information (SI), Section 1), we identified a threshold in parameter space where the homogeneous steady state becomes unstable and a stable limit cycle (sustained oscillations) emerges. Our analysis reveals that within the parameter space defined by  $k'_a$ ,  $k'_d2$  and  $k'_d3$  (Fig. 2), the system has two distinct regions separated by a stability boundary (surface). In the region where the real part of the complex-conjugate eigenvalue pair is positive, the steady state is unstable, and perturbations grow over time. Conversely, when the real part is negative, the steady state is stable, and perturbations decay exponentially with time. This analysis provides a map of the parameter space, showing the transition from stable to unstable regimes. In particular, as the monomer activation rate or other rate constants exceed critical values, the system undergoes

a Hopf bifurcation, the onset of oscillatory behavior characterized by periodic cycles of polymer mass growing and shrinking<sup>36</sup>. Numerically, we find that beyond the bifurcation surface the system relaxes to a stable steady state (with damped oscillations), whereas within it the concentration of the monomer and polymer species enter sustained oscillatory cycles as depicted in Fig. 2. These observations suggest that sustained oscillations result from a feedback interplay between autocatalytic growth and delayed inhibitory processes.

#### 3.2 Kinetic parameters tune polymer length and system dynamics

We first examine how the rate constants  $k'_a$  (monomer activation),  $k'_d2$  (polymer-end deactivation), and  $k'_d3$  (polymer chain-deactivation) influence the average polymer length at steady state in the oscillatory region of the parameter space, defined as  $L_{ss} = m_1^*/m_0^*$  (Fig. 3a). To enable direct comparison, each rate constant is varied independently while the others are fixed, and all are rescaled by their respective reference values.

An increase in the activation rate constant  $k'_a$  leads to longer supramolecular polymers, as activated monomers are rapidly incorporated into growing chains, increasing both polymer number and mass without significantly altering the total activated monomer concentration. In contrast, higher polymer-end deactivation rates ( $k'_d2$ ) decrease both polymer number and mass but reduce the polymer number more strongly, resulting in a

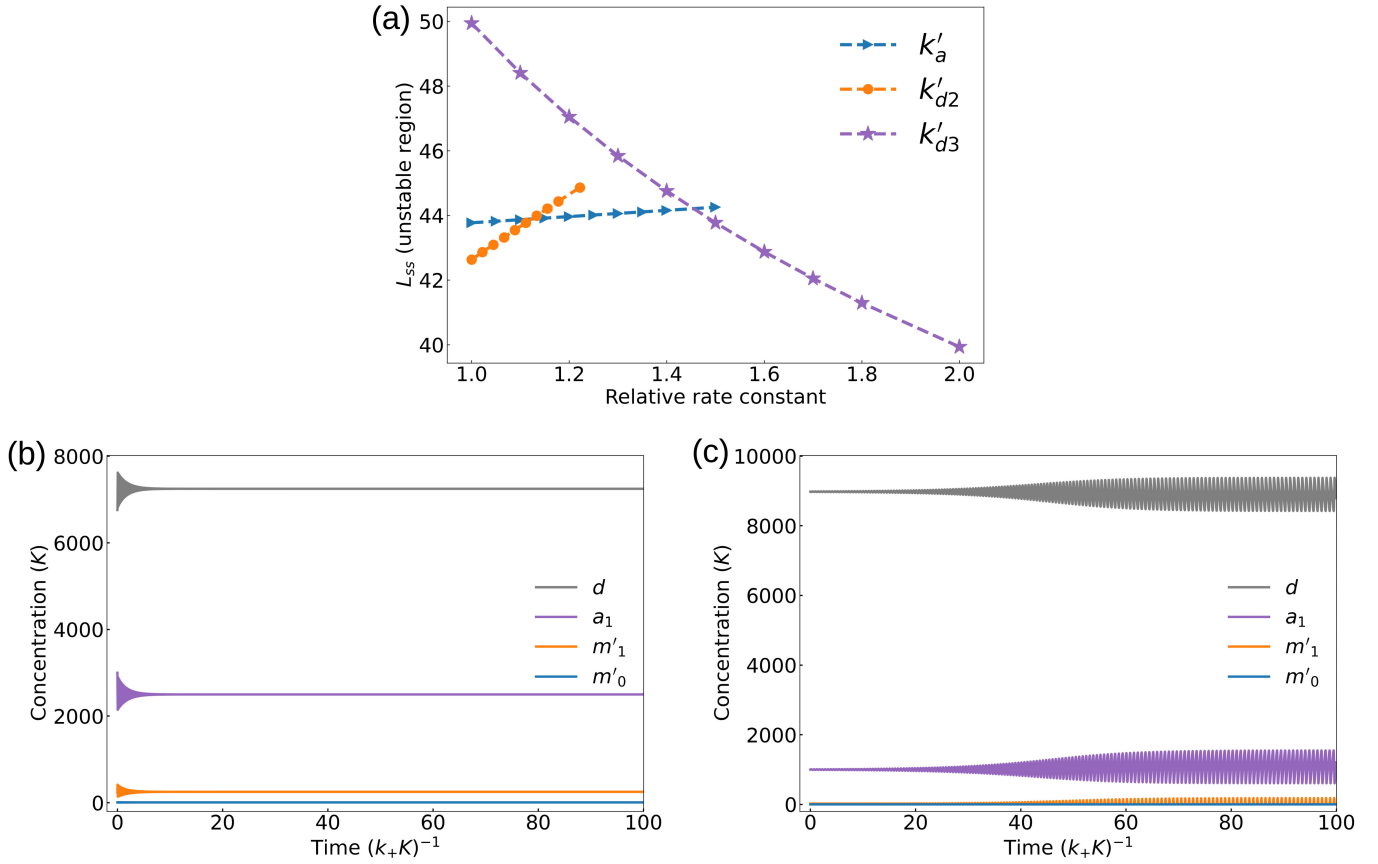


Fig. 3 (a) Variation of the steady-state average polymer length within the unstable regime upon changing a single parameter, while keeping the remaining two parameters fixed. The data are shown for  $k'_a$  ranging from 4 to 6,  $k'_{d2}$  from 4600 to 5300, and  $k'_{d3}$  from 0.55 to 0.9. All rate constants are rescaled by their corresponding initial value in each plot. (b) Numerical simulation results showing the temporal evolution of  $d(t)$ ,  $a_1(t)$ ,  $m'_1(t)$ , and  $m'_0(t)$  at a representative point in the stable region ( $k'_a = 5$ ,  $k'_{d2} = 2500$ ,  $k'_{d3} = 1.005$ ). (c) Temporal evolution of the same variables at a representative point in the unstable region ( $k'_a = 0.2$ ,  $k'_{d2} = 1000$ ,  $k'_{d3} = 1$ ).

net increase in the average polymer length. Increasing the chain-deactivation rate ( $k'_{d3}$ ) fragments long chains into shorter ones, thereby increasing polymer number while decreasing overall polymer mass, leading to shorter average lengths.

To probe the system's dynamic behavior, we numerically integrate the reduced kinetic equations (see Methods section and SI, Section-2). For parameters within both the stable and unstable regions of the phase diagram, the temporal evolution of  $d(t)$ ,  $a_1(t)$ ,  $m'_1(t)$ , and  $m'_0(t)$  displays oscillatory behavior. In the stable regime, these oscillations are damped and relax to steady-state values (Fig. 3b), while in the unstable regime, they evolve into a sustained limit cycle (Fig. 3c). The transition between these regimes occurs via a Hopf bifurcation, marking the onset of autonomous temporal oscillations. This kinetic instability motivates further exploration of how diffusive coupling alters the spatiotemporal dynamics of the system.

### 3.3 Emergence of self-organized wavefronts and patterns

To explore spatiotemporal instability leading to self-organized pattern formation in the supramolecular polymerization system as described by the kinetic model (Eqns. 1-4), we extend the ki-

netic model by incorporating diffusion to account for transport processes. Diffusion is described using the Rouse-type scaling<sup>37</sup>, which provides a simple and physically meaningful representation of polymer dynamics in dilute, unentangled systems<sup>38,39</sup>. According to this model, the diffusion coefficient of a polymer decreases inversely with its length, making it particularly suitable for supramolecular polymers that are transient, unentangled, and formed under dilute conditions. Coupling this length-dependent diffusion with the nonlinear reaction kinetics leads to emergent spatiotemporal phenomena such as traveling fronts and complex pattern formation. The resulting reaction-diffusion equations for the four species: deactivated monomers ( $d$ ), activated monomers ( $a_1$ ), total polymer mass concentration ( $m'_1$ ), and total polymer number concentration ( $m'_0$ )—are given by:

$$\dot{d} = -k'_a d + 2k'_{d2} m'_0 + D_0 \nabla^2 d, \quad (5)$$

$$\dot{a}_1 = k'_a d - 2k_+ a_1 m'_0 + D_0 \nabla^2 a_1, \quad (6)$$

$$\dot{m}'_1 = -2k'_{d2} m'_0 + 2k_+ a_1 m'_0 + \vec{\nabla} (D_m \vec{\nabla} m'_1), \quad (7)$$

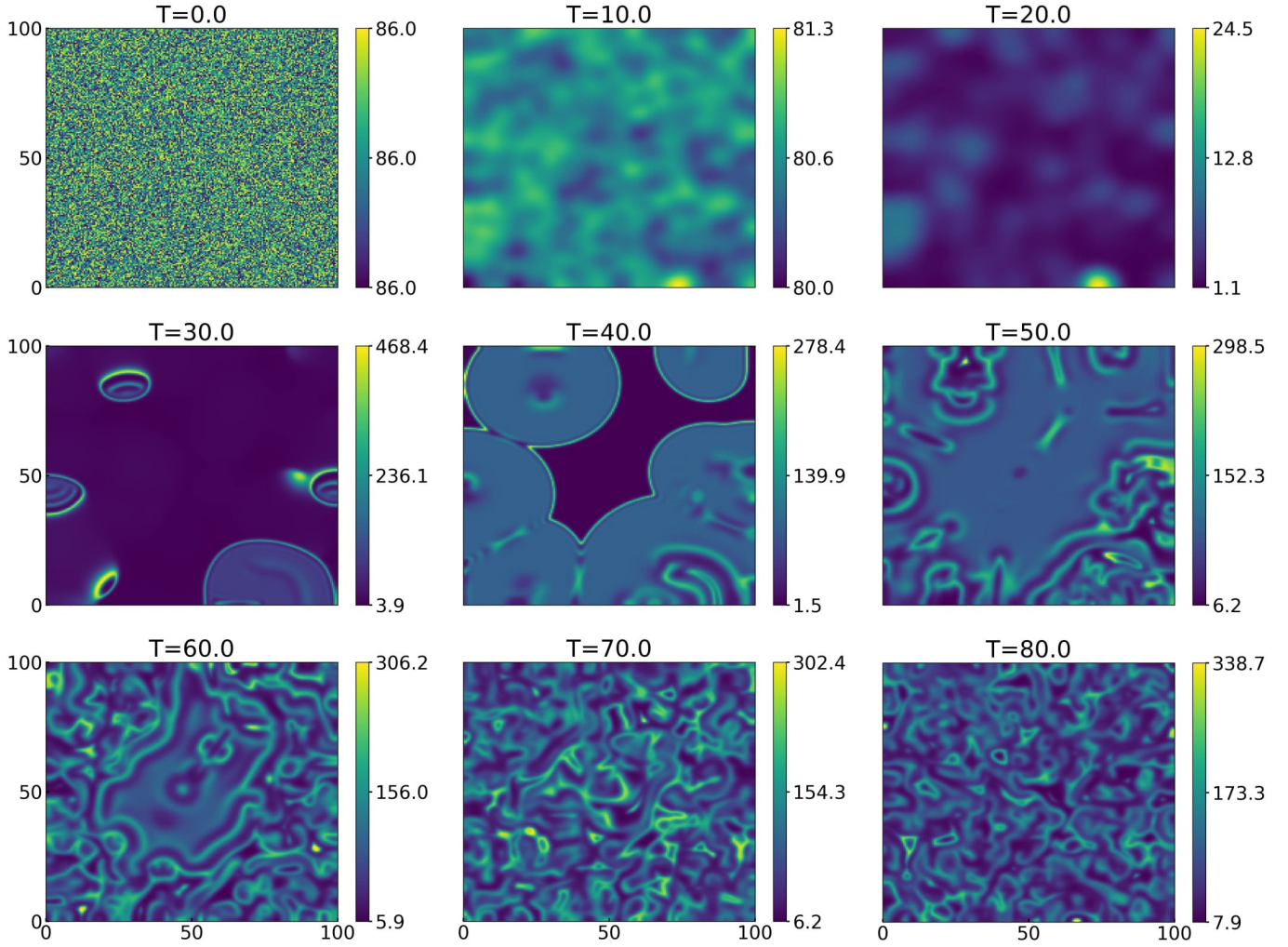


Fig. 4 Snapshots of the polymer mass concentration at different times during the spatiotemporal simulation for a parameter set located in the oscillatory region ( $k'_a = 4.0$ ,  $k'_{d2} = 5000.0$ , and  $k'_{d3} = 1.5$ ), initialized with random perturbations. Domain size is  $100 \times 100$ . Grid size is 0.5. Time is expressed in units of  $(k_+ K)^{-1}$ .

$$\dot{m}'_0 = k'_{d3}(m'_1 - 4m'_0) - \frac{2k'_{d2}Cm'_0}{(m'_1/m'_0 - 2)^2} - 2k'_{d3}m'_0 - k_+(m'_0)^2 + \vec{\nabla}(D_m \vec{\nabla} m'_0). \quad (8)$$

Here,  $D_0$  and  $D_m$  denote the diffusion coefficients of monomers and polymers, respectively. Following the Rouse scaling, the polymer diffusion coefficient depends on its instantaneous average length,  $L_p = m'_1/m'_0$ , such that  $D_m = D_0/L_p$ . The monomer diffusion coefficient is fixed at  $D_0 = 1.0$  in the dimensionless units defined in the section Model description. This formulation is not merely a technical detail but a crucial physical ingredient of the model. In supramolecular polymer systems, chemical reactions and diffusion are intimately coupled: polymerization locally reduces molecular mobility, while depolymerization enhances it. By incorporating length-dependent diffusivity, the model captures this feedback between structure formation and mass transport, allowing for dynamic spatial heterogeneity to emerge self-consistently. Regions with higher polymer content experience reduced diffusion, which can stabilize concentration gradients and give rise to front propagation, wave formation, or pattern lo-

calization. Conversely, when depolymerization dominates, the increased mobility can erase gradients, restoring homogeneity. This interplay between reaction kinetics and diffusion provides a mechanistic basis for spatial self-organization, analogous to the spatial instability or reaction-diffusion mechanisms observed in biological systems.

Importantly, the inclusion of Rouse-type diffusion scaling grounds the model in physical polymer theory, distinguishing it from purely phenomenological reaction-diffusion models with constant diffusivities. It enables a direct link between molecular-scale dynamics (e.g., polymer growth, fragmentation) and macroscopic pattern evolution, thereby enhancing the model's predictive power. Such coupling between chain length and diffusivity is expected to be a general feature of fuel-driven supramolecular assemblies, where local variations in assembly state modulate effective transport properties. By capturing this essential coupling, our framework provides a more realistic and physically consistent route to understanding and predicting the emergence of spatiotemporal order in active supramolecular materials.

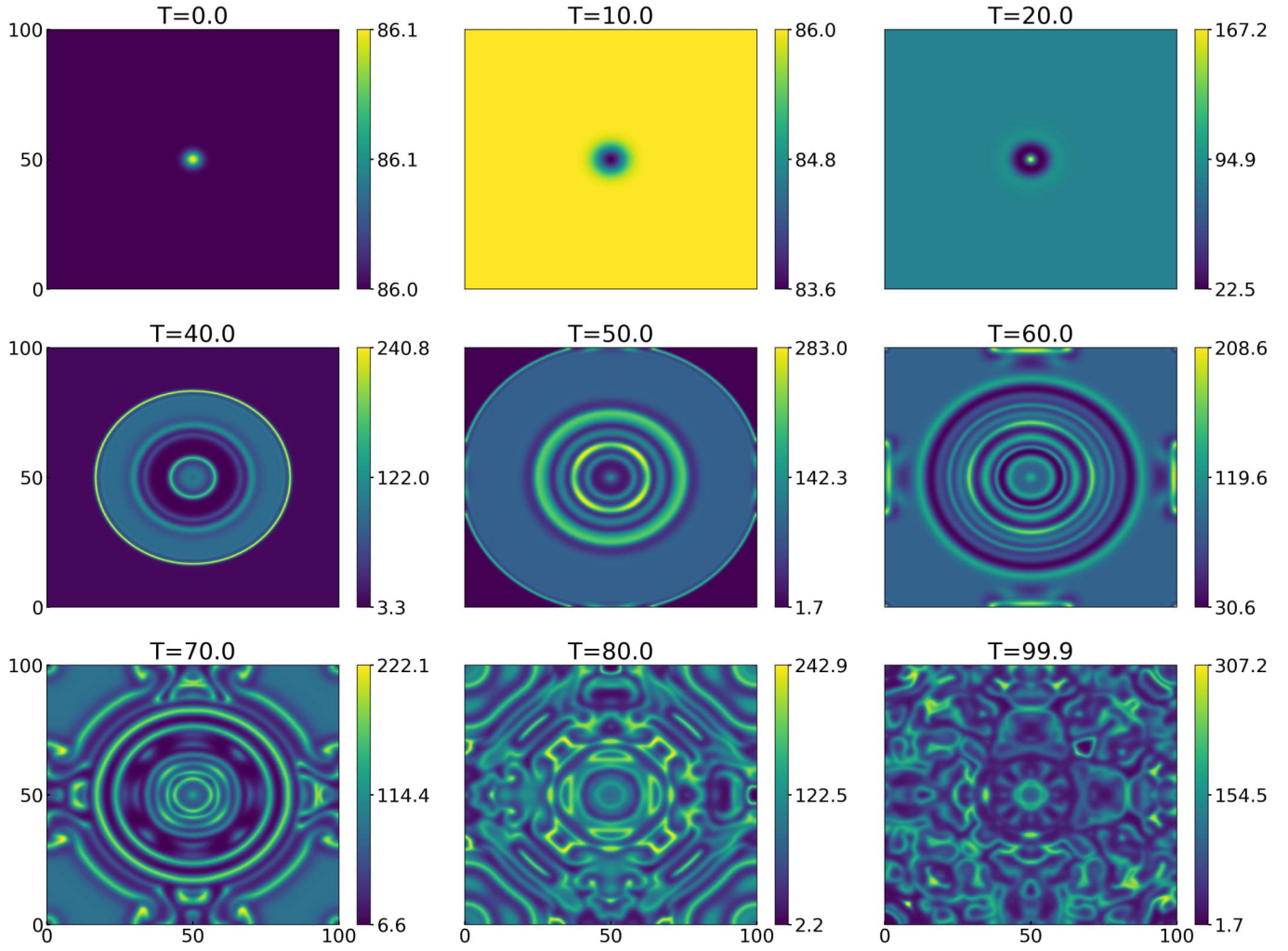


Fig. 5 Snapshots of the polymer mass concentration at different times during the spatiotemporal simulation for a parameter set in the limit-cycle regime ( $k'_a = 4.0$ ,  $k'_{d2} = 5000.0$ , and  $k'_{d3} = 1.5$ ), initiated using a Gaussian perturbation. Domain size is  $100 \times 100$ . Grid size is 0.1. Time is expressed in units of  $(k_+ K)^{-1}$ .

Taking a representative point described by parameters:  $k'_a = 4.0$ ,  $k'_{d2} = 5000.0$ , and  $k'_{d3} = 1.5$ , within the oscillatory region of the parameter space, we numerically integrated the two-dimensional reaction-diffusion equations after introducing a small random initial perturbation drawn from a uniform distribution (see Methods section and SI-Section-2). Initially, the system exhibits a nearly homogeneous state with no discernible spatial variations. Over time, however, random patches of elevated polymer concentration transiently appear and disappear. At later times, localized regions of higher polymer density serve as nucleation centers that propagate outward as traveling wavefronts. These wavefronts expand, interact, and eventually merge, leading to the emergence of transient polygon-like spatial patterns at longer times (Fig. 4). The corresponding pattern evolution is demonstrated in Movie-S1 (in SI, Section-3). Similar wavefront propagation phenomena have been experimentally reported in fuel-driven supramolecular systems<sup>19,29</sup>. When the same analysis is performed for a parameter set within the stable region, no spatial pattern formation is observed. In this regime, the homogeneous steady state

remains strongly stable, and diffusion alone cannot destabilize it. The emergence of spatiotemporal organization in the limit-cycle regime thus arises from the nonlinear coupling between reaction kinetics and diffusion of the interacting species. This interplay gives rise to self-organized traveling polymer mass fronts and complex transient spatial morphologies characteristic of active supramolecular materials.

To further examine the dynamics of traveling wavefronts, we introduce a localized Gaussian perturbation to the polymer mass concentration ( $m'_1$ ) and polymer number concentration ( $m'_0$ ) at the center of the spatial domain. This Gaussian perturbation serves as a controlled and localized seed, enabling a systematic investigation of wavefront initiation and propagation in the system. The resulting traveling wavefronts exhibit intricate internal structures, characterized by multiple concentric rings of alternating high and low concentration regions that continuously emerge and dissipate within the propagating front. Interestingly, regions outside the advancing front occasionally display polymer mass concentrations higher than those within the front

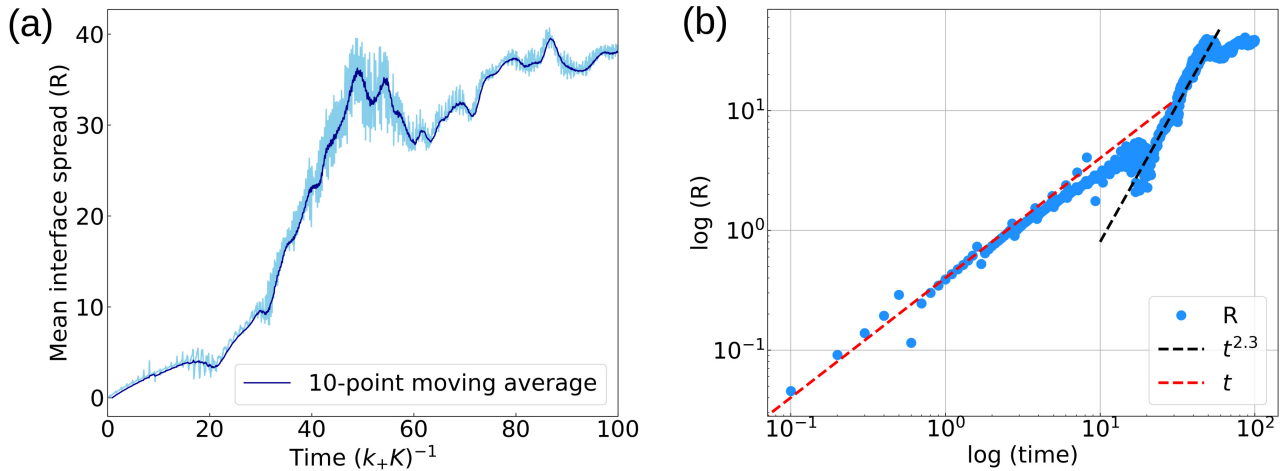


Fig. 6 (a) Temporal evolution of the interface spread for a Gaussian-perturbed system at  $k'_a = 4.0$ ,  $k'_{d2} = 5000.0$ , and  $k'_{d3} = 1.5$ . (b) Power-law scaling of the interface spread with time for the same parameter set, showing two distinct regimes: linear and accelerated growth.

boundary. These features arise from the nonlinear coupling and feedback inherent in the reaction network, which governs the activation-deactivation and assembly-disassembly processes. At longer times, the system evolves into transient polygon-like spatial patterns, consistent with those observed under random perturbations (Fig. 5). The corresponding pattern evolution is further illustrated in Movie-S2 (see SI, Section-3). In addition, we explored multiple points across the parameter space and present the spatiotemporal dynamics of a representative parameter set ( $k'_a = 0.9$ ,  $k'_{d2} = 2000.0$ , and  $k'_{d3} = 0.1$ ) located close to the bifurcation surface in Movie S3 (SI, Section-3). The qualitative nature of the wave dynamics closely resembles that observed deep within the spatiotemporally unstable domain. To quantify this behavior and extract scaling properties, we analyze the dynamics of the moving interface in detail.

### 3.4 Accelerated wavefront propagation

To analyze the propagation of traveling fronts quantitatively, we introduced a single localized perturbation: a small seed of polymer-rich region into an otherwise homogeneous oscillatory system. This perturbation initiates a radially expanding polymerization wave, enabling direct measurement of the front's propagation dynamics over time (Fig. 6a).

To quantify the propagation of the wavefront, we compute the gradient field of the polymer mass concentration,

$$g = \nabla m'_1$$

evaluated at every spatial point and at each timestep. Tracking the interface of the gradient field, quantified through  $R(t)$ , reveals that the front expansion is not constant in time. The detailed procedure for computing the gradient field and extracting  $R(t)$  is provided in SI, Section 4. Initially, the wavefront grows linearly, indicating propagation at an approximately constant speed. At later times, however, the front exhibits accelerated spreading, marking the onset of a distinct nonlinear growth regime. Quantitatively, the interface spread follows a power-law scaling relation,

$R(t) \sim t^p$ , where the exponent  $p$  increases from  $\sim 1$  in the early stage to value  $\sim 2.3$  at later times (Fig. 6b). Notably, when the same analysis is performed for a parameter set located closer to the bifurcation surface ( $k'_a = 0.9$ ,  $k'_{d2} = 2000$ , and  $k'_{d3} = 0.1$ ) the late-time growth is significantly weaker, yielding a reduced exponent of  $\sim 1.3$ , while the initial linear scaling remains unchanged. The result is shown in Fig. S1. This sensitivity of the scaling exponent to proximity to the bifurcation highlights the tunable nature of wavefront dynamics in the system. This accelerated propagation indicates super-diffusive spreading of the polymerization front, far faster than what would be expected from normal diffusion and reflects the inherently nonlinear nature of the underlying reactive dynamics. The acceleration arises because the medium behind the propagating front continues to oscillate and periodically generates secondary waves that reinforce the leading front, thereby enhancing the overall propagation speed. This self-reinforcing mechanism reflects the interplay between chemical feedback and diffusion-driven transport in the active supramolecular system.

This quantitative framework provides predictive relationships between reaction kinetics and pattern dynamics, offering experimentally testable hypotheses. For instance, analogous scaling behavior might be observed in chemically fueled gels or active supramolecular materials, where the apparent front speed could depend on fuel concentration or catalyst activity. Such scaling laws extend beyond qualitative pattern observation, providing a direct bridge between measurable dynamic fronts and the underlying non-equilibrium chemistry.

### 3.5 Patterns are robust to system size and resolution

To assess the robustness of the observed spatiotemporal dynamics, we examined the influence of both the system size and the numerical grid resolution (see SI, Section-5). Simulations performed on a spatial domain twice as large as that used in the main analysis show that increasing the domain size primarily affects boundary-related features. Larger systems support the formation

of a greater number of polymerization seeds under random perturbations and allow Gaussian-triggered wavefronts to propagate for longer durations before interacting with the boundaries. Importantly, apart from these finite-size effects, the qualitative features of the dynamics, including wavefront initiation, propagation, and decay remain unchanged. Representative results are provided in the Supporting Information (Figs. S2 and S3).

We further examined the effect of spatial discretization by varying the grid spacing while keeping all other parameters fixed. For simulations initiated with a central Gaussian perturbation, coarser grids ( $\Delta x = \Delta y = 0.5$ ) lead to earlier symmetry breaking and increased anisotropy of the expanding wavefronts compared to finer grids ( $\Delta x = \Delta y = 0.1$ ) as shown in Fig. S4. This behavior arises from numerical discretization effects rather than changes in the underlying reaction-diffusion mechanism. Consistently, employing higher-order spatial discretization schemes (e.g., nine-point stencils) delays the onset of symmetry breaking and preserves circular wavefronts over longer times (Fig. S5). These observations confirm that the reported spatiotemporal patterns are intrinsic to the model and remain robust across system sizes and numerical resolutions.

### 3.6 Connecting model predictions with experimental observations

Despite its minimal structure, the present reaction-diffusion model successfully captures the core dynamical phenomena, autonomous oscillations, traveling polymerization fronts, and complex pattern formation reported in experimental studies of chemically fueled supramolecular polymerization<sup>19</sup>. Both the experiments and our theoretical model rely on a fundamental interplay between an autocatalytic growth (fragmentation-mediated feedback) process and a slower deactivation step, thereby satisfying the classical conditions required for self-sustained oscillations in open, driven systems<sup>1,40</sup>.

A notable difference, however, lies in the mechanism of pattern formation. In experiments, centimeter-scale convection-driven patterns often arise due to density variations accompanying monomer assembly, whereas in the present model, the emergence of spatial structure results purely from a two-dimensional reaction-diffusion setting in the absence of any convective flow. This distinction suggests that, in experimental settings, convection could either be minimized such as by immobilizing the system within a gel or microfluidic device to realize only diffusion-dominated patterning, or alternatively harnessed to amplify mesoscale organization across larger length scales.

Moreover, the model framework enables systematic variation of kinetic parameters and the construction of a quantitative phase diagram that delineates transitions between steady and oscillatory regimes. Such detailed exploration is typically challenging to achieve experimentally. Our analysis predicts that modifying key rates such as monomer activation or polymer-chain deactivation can tune the system across the Hopf bifurcation boundary, thereby controlling whether the system exhibits steady-state or oscillatory behavior. These insights provide direct design guidelines for future experiments, for instance by adjusting fuel concentration or

molecular design to modulate fragmentation kinetics.

In essence, the present theoretical framework complements experimental efforts by providing a controllable and computationally accessible platform to explore “what-if” scenarios. It reveals emergent behaviors such as multi-ring wavefront structures and tunable super-diffusive scaling laws that have not yet been explicitly observed in experiments, but could be tested in future studies. Together, these findings strengthen the connection between minimal non-equilibrium modeling and real dissipative self-assembly, advancing our understanding of how simple kinetic motifs can give rise to rich spatiotemporal organization.

## 4 Conclusions and Outlook

The emergence of self-organized patterns in dissipative supramolecular systems has become a central theme in systems chemistry, offering a chemical route to life-like spatiotemporal organization<sup>19,41</sup>. In this work, we introduced a minimal reaction-diffusion model for a fuel-driven supramolecular polymerization system, capturing essential features of activation-deactivation chemistry coupled to cooperative polymer growth and fragmentation. Despite its conceptual simplicity, the model reproduces a broad spectrum of experimentally relevant behaviors, including autonomous oscillations, propagating wavefronts, and complex self-organized spatial structures.

A major challenge in modeling such systems lies in the coexistence of nonlinear reaction kinetics with the spatial transport of both monomers and polydisperse polymeric species. Our framework addresses this by explicitly incorporating length-dependent diffusion, following Rouse scaling, thereby providing a physically grounded representation of polymer mobility. Monomers diffuse faster than polymer aggregates, an asymmetry that proves crucial for pattern formation.

Through linear stability analysis of the temporal model, we systematically mapped the three-dimensional parameter space and identified the bifurcation surface separating stable steady states from oscillatory regimes. The onset of oscillations occurs via a Hopf bifurcation, in agreement with the numerical simulations. Upon incorporating diffusion, these temporal oscillations extend into rich spatial dynamics, giving rise to traveling fronts and transient polygonal and wave-like patterns. The spatially resolved simulations not only reproduce qualitative phenomenology but also enable quantitative characterization of front propagation, including scaling laws and the emergence of nonlinear spreading regimes.

Overall, this work highlights how autocatalytic assembly coupled with inhibitor-mediated disassembly, when embedded within a spatially extended reactive medium, is sufficient to generate diverse spatiotemporal behaviors reminiscent of biological nonequilibrium systems. By revealing the mechanistic routes through which minimal chemical reaction networks can support oscillations and pattern formation, our model contributes to a growing theoretical foundation for designing programmable, fuel-driven supramolecular materials. It underscores the broader principle that temporal and spatial order can arise spontaneously from simple chemical rules, a hallmark of systems operating far from equilibrium.

This minimal framework establishes a foundation for systematic exploration of active supramolecular systems. Future work may include incorporating various external or internal perturbations such as advective fields, hydrodynamic coupling, energy dissipation and entropy production analysis, or stochastic fluctuations to bridge kinetics with thermodynamic irreversibility. Experimental validation of the predicted accelerated front propagation, multi-ring wave structures, or spatiotemporal scaling laws would further solidify the model's relevance and inspire new experimental designs. Ultimately, the ability to simulate and predict biological-like dynamics using simple chemical rules brings us closer to the creation of life-like materials such as autonomous chemical systems capable of adaptation, communication, and function. This study thus contributes not only to the theoretical understanding of dissipative supramolecular polymerization, but also to the broader pursuit of self-organizing, self-regulating matter in chemistry and materials science.

## Methods

### Linear Stability Analysis

We performed linear stability analysis to determine the conditions under which the spatially homogeneous steady state becomes unstable. Using mass conservation, the original four-variable simplified kinetic model was reduced to an equivalent three-variable system. The homogeneous steady state was obtained by solving the resulting nonlinear algebraic equations, and the Jacobian matrix was evaluated at this state. The stability of the system was determined by numerically computing the eigenvalues of the Jacobian matrix for the homogeneous steady state for different parameter values. The steady state was classified as stable when all eigenvalues had negative real parts, while a Hopf bifurcation was identified when a complex-conjugate pair crossed the imaginary axis, indicating the onset of oscillatory dynamics. Further details are provided in Supplementary information, Section-1.

### Numerical Integration and Wavefront Analysis

We numerically integrated the temporal reaction kinetics to characterize system dynamics across stable and oscillatory regimes. Simulations were initialized at the homogeneous steady state with small perturbations. Time evolution was computed using a forward Euler scheme with a timestep  $\Delta t = 10^{-4}$  and a total integration time  $t_{max} = 100$ . To study spatial effects, the model was extended to a two-dimensional reaction-diffusion system. Simulations were performed on a square domain with zero-flux boundary conditions and random initial perturbations. The local diffusion coefficients of the polymer number and polymer mass concentrations were updated dynamically based on the instantaneous polymer length, whereas the monomer (activated and deactivated) diffusion coefficients were kept constant. Traveling wavefront behavior was further investigated by introducing localized Gaussian perturbations at the center of the domain. To quantify wave propagation, we computed the gradient of the polymer mass concentration and tracked the spatial spread of this field to define a root-mean-square radius  $R(t)$ . The temporal scaling of  $R(t)$  was obtained by fitting its time dependence to a power-law

relation (more information is provided in Supplementary information, Sections 2 and 4).

## Author contributions

**Akta Singh:** Conceptualization, Methodology, Formal Analysis, Investigation, Writing- original draft. **Nayana Mukherjee:** Conceptualization, Methodology, Formal Analysis, Investigation. **Jagannath Mondal:** Conceptualization, Supervision, Funding acquisition, Writing- original draft. **Pushpita Ghosh:** Conceptualization, Methodology, Formal Analysis, Investigation, Supervision, Funding acquisition, Writing- original draft.

## Conflicts of interest

The authors have no conflicts to declare.

## Data availability

The data supporting this article have been included as part of the Supplementary Information.

## Supporting Information

The Supporting Information (SI) provides additional figures (Figs. S1-S5) and supplementary movies S1-S3 mentioned in the main text, along with supplementary methods and technical details that support the findings of this manuscript.

## Acknowledgements

The authors acknowledge the Tata Institute of Fundamental Research Hyderabad, and the Indian Institute of Science Education and Research Thiruvananthapuram, India, for providing computing resources. We acknowledge support from the Department of Atomic Energy, Government of India, under Project Identification No. RTI 4007. A.S. thanks Hriley Narula, Roshan Maharana, and Purnima Jain for useful discussions.

## Notes and references

- 1 I. R. Epstein and J. A. Pojman, *An introduction to nonlinear chemical dynamics: oscillations, waves, patterns, and chaos*, Oxford University Press, 1998.
- 2 J. D. Murray, *Mathematical Biology*, 2003.
- 3 M. Cross and H. Greenside, *Pattern formation and dynamics in nonequilibrium systems*, Cambridge University Press, 2009.
- 4 E. Karsenti, *Nature reviews Molecular cell biology*, 2008, **9**, 255–262.
- 5 J. Halatek and E. Frey, *Nature Physics*, 2018, **14**, 507–514.
- 6 B. Alberts, A. Johnson, J. Lewis, D. Morgan, M. Raff, K. Roberts and P. Walter, *Molecular Biology of the Cell*, W. W. Norton & Company, New York, 7th edn, 2022.
- 7 H. Hess and J. L. Ross, *Chemical Society Reviews*, 2017, **46**, 5570–5587.
- 8 K. C. Huang, Y. Meir and N. S. Wingreen, *Proceedings of the National Academy of Sciences*, 2003, **100**, 12724–12728.
- 9 B. Bugyi and M.-F. Carlier, *Annual review of biophysics*, 2010, **39**, 449–470.
- 10 R. Dominguez and K. C. Holmes, *Annual review of biophysics*, 2011, **40**, 169–186.

11 G. J. Brouhard and L. M. Rice, *Nature reviews Molecular cell biology*, 2018, **19**, 451–463.

12 A. Akhmanova and L. C. Kapitein, *Nature Reviews Molecular Cell Biology*, 2022, **23**, 541–558.

13 E. Mandelkow, E.-M. Mandelkow, H. Hotani, B. Hess and S. C. Müller, *Science*, 1989, **246**, 1291–1293.

14 K. Mondal, T. Maiti and P. Ghosh, *Journal of Chemical Theory and Computation*, 2025, **21**, 4405–4416.

15 S. De and R. Klajn, *Advanced Materials*, 2018, **30**, 1706750.

16 S. Dhiman and S. J. George, *Bulletin of the Chemical Society of Japan*, 2018, **91**, 687–699.

17 M. G. Howlett, A. H. Engwerda, R. J. Scanes and S. P. Fletcher, *Nature Chemistry*, 2022, **14**, 805–810.

18 G. Ragazzon and L. J. Prins, *Nature Nanotechnology*, 2018, **13**, 882–889.

19 J. Leira-Iglesias, A. Tassoni, T. Adachi, M. Stich and T. M. Hermans, *Nature Nanotechnology*, 2018, **13**, 1021–1027.

20 A.-D. C. Nguindjel, P. J. de Visser, M. Winkens and P. A. Korevaar, *Phys. Chem. Chem. Phys.*, 2022, **24**, 23980–24001.

21 X.-F. Hou, X. Chen, J.-H. Wei, Y. Xu, X.-M. Chen and Q. Li, *Responsive Materials*, 2023, **1**, e20230016.

22 X. Lang, Y. Huang, L. He, Y. Wang, U. Thumu, Z. Chu, W. T. Huck and H. Zhao, *Nature Communications*, 2023, **14**, 3084.

23 J. Li, Y. Cui, Y.-L. Lu, Y. Zhang, K. Zhang, C. Gu, K. Wang, Y. Liang and C.-S. Liu, *Nature Communications*, 2023, **14**, 5030.

24 J. Boekhoven, W. E. Hendriksen, G. J. Koper, R. Eelkema and J. H. van Esch, *Science*, 2015, **349**, 1075–1079.

25 R. D. Astumian, *Nature Communications*, 2019, **10**, 3837.

26 R. Merindol and A. Walther, *Chemical Society Reviews*, 2019, **48**, 4136–4177.

27 S. A. P. van Rossum, M. Tena-Solsona, J. H. van Esch, R. Eelkema and J. Boekhoven, *Chemical Society Reviews*, 2017, **46**, 5519–5535.

28 A. Sharko, D. Livitz, S. De Piccoli, K. J. M. Bishop and T. M. Hermans, *Chemical Reviews*, 2022, **122**, 11759–11777.

29 R. Kubota, M. Makuta, R. Suzuki, M. Ichikawa, M. Tanaka and I. Hamachi, *Nature communications*, 2020, **11**, 3541.

30 T. Nagai, T. Fukui, D. Koda, K. Mawatari, S. Takeuchi and T. Sugawara, *Nature Communications*, 2021, **12**, 4486.

31 E. te Brinke, J. Groen, A. Herrmann, H. A. Heus, G. Rivas, E. Spruijt and W. T. S. Huck, *Nature Nanotechnology*, 2018, **13**, 849–855.

32 M. Tena-Solsona, B. Rieß, R. K. Grötsch, F. C. Löhrer, C. Wanzke, B. Käsdorf, A. R. Bausch, P. Müller-Buschbaum, O. Lieleg and J. Boekhoven, *Nature Communications*, 2017, **8**, 15895.

33 G. Fichman, L. A. Serrano, S. Dhiman, A. Estévez-Torres and T. M. Hermans, *Advanced Materials*, 2021, **33**, 2008436.

34 D. Mandal, S. Dhiman and S. J. George, *Accounts of Chemical Research*, 2023, **56**, 2310–2323.

35 S. Bal, K. Das, S. Ahmed and D. Das, *Angewandte Chemie International Edition*, 2019, **58**, 244–247.

36 S. K. Scott, *Oscillations, waves, and chaos in chemical kinetics*, Oxford University Press, 1994.

37 P. E. Rouse, *The Journal of Chemical Physics*, 1953, **21**, 1272–1280.

38 M. Doi and S. F. Edwards, *The Theory of Polymer Dynamics*, Oxford University Press, 1986.

39 M. Rubinstein and R. H. Colby, *Oxford University Press*, 2003.

40 G. Nicolis and I. Prigogine, *Self-Organization in Nonequilibrium Systems*, Wiley, New York, 1977.

41 A. Walther, *Advanced Materials*, 2020, **32**, 1905111.